

Supporting information for

Gold nanoparticle hybridized rubrene nanofibers made by electrospinning: Enhancement of optical and structural properties

Krishna P. Dhakal,^{a,b} Hyunsoo Lee,^{a,b} Jubok Lee,^{a,b} Seok Ho Lee,^c Jinsoo Joo^{c,*} and Jeongyong Kim^{a,b*}

^aDepartment of Energy Science, Sungkyunkwan University, Suwon 440-746, Korea.

^bIBS Center for Integrated Nanostructure Physics, Institute for Basic Science (IBS), Daejon 305-701, Korea.

^c Department of Physics, Korea University, Seoul 136-713, Korea.

*Corresponding author. E-mail: j.kim@skku.edu, phone: +82-(0)31-299-4054 (O), Fax: +82-(0)31-299-4279

*Corresponding author. E-mail: jjoo@korea.ac.kr

This Supporting Information presents the following results:

- I. Preparation of the dodecanethiol functionalized Au NPs and electrospinning of the rubrene NFs and hybrid rubrene NFs.
- II. Porous size distribution on the hybrid rubrene NF.
- III. Finite difference time domain (FDTD) simulation result of the light absorption and scattering due to porous effect on the hybrid rubrene NFs.
- IV. EDX analysis from the TEM image of the hybrid rubrene NF.
- V. IR spectroscopy of rubrene NFs and hybrid rubrene NFs.

I. Preparation of the dodecaethiol functionalized gold nanoparticles and electrospinning of the rubrene NFs and hybrid rubrene NFs

Dodecanethiol functionalized gold nanoparticles (Au NP) of size 3 nm dissolved in chloroform were prepared at room temperature (rt) by reducing gold (III) derivatives, based on the previously mentioned method by Leff *et al.*¹ and Kim *et al*². In brief, approximately 15 mL of a bright yellow 0.0305 M (0.458 mmol) HAuCl₄H₂O (Sigma Aldrich, 99.99%) (aq) solution was added to an empty glass reaction vessel. 10.20 mL of a 0.0999 M (1.02 mmol) N (C₈H₁₇)₄-Br (TCI America, 98%) solution in toluene was added as a phase-transfer (aqueous to organic) reagent. In the organic phase, 3.13 mL of a 0.0418 M (0.131 mmol) C₁₂H₂₅SH (Sigma Aldrich, 98%) solution in toluene was added, which was followed by the addition of 12.5 mL of 0.0418 M (5.03 mmol) NaBH₄ (Sigma Aldrich, 98%) aqueous solution in order to reduced the gold chloride. There was an instant color change of the organic phase to the purple color, and then eventually to the black/brown color. Then the solution was left open to the atmosphere for approximately 6 hour, while being rapidly stirred. And then the organic phase was separated from the aqueous phase. The organic phase was then added in the 350 mL of 95% ethanol and kept at temperature ~ -10°C for 4 hour for the precipitation to occur. The dark black/brown precipitate was then filtered with 200 nm pore-size filter paper (Whatman), and washed with 95% ethanol. The filtrate was dried in a vacuum, and 70-80 mg of Au NPs powder was obtained, which was directly used to prepare the electrospinning solution for hybrid rubrene NFs. Different concentration of the Au NPs was maintained in preparing hybrid rubrene NFs and optical properties were compared with the plane rubrene NFs made in the same condition. The amount of gold nanoparticles used to prepare the solution for hybrid rubrene NFs were 2.5 wt.%, 5 wt.%, 10 wt.%, 15 wt.%, 20 wt.%, 25 wt.% and 30 wt.% of the rubrene weight in the reaction mixture.

The solution for the rubrene NFs and hybrid rubrene NFs were prepared in chloroform using the materials rubrene (99.99 %), PEO (99.99 %) and Au NPs powder. Rubrene and PEO were dissolved in chloroform with their weights in the ratio of 10:1 and the solution for the rubrene NFs was prepared similar to the previously reported report on preparation of rubrene NFs.³ Solution for the hybrid rubrene NFs was also prepared dissolving the same amount of rubrene and PEO as used to prepare solution for rubrene NF plus Au NPs in the reaction mixture with chloroform.

Nanofibers were prepared using the known electrospinning process using a manufactured electrospinner (Nano NC Corp.) Solution of the rubene NF or hybrid NF was injected into 12 mL syringe having the small diameter (0.4mm) needle with the high electrical bias. The droplet of the solution coming out of the needle, with high voltage electric bias, was converted into the, so called, Taylor cone and finally stretched as long and continuous nanofibers. In our experiment we used electrospinning equipment (Nano NC) with the setup of with a 0.4 mm diameter needle. the schematic for electrospinning is shown in Fig. S₁.

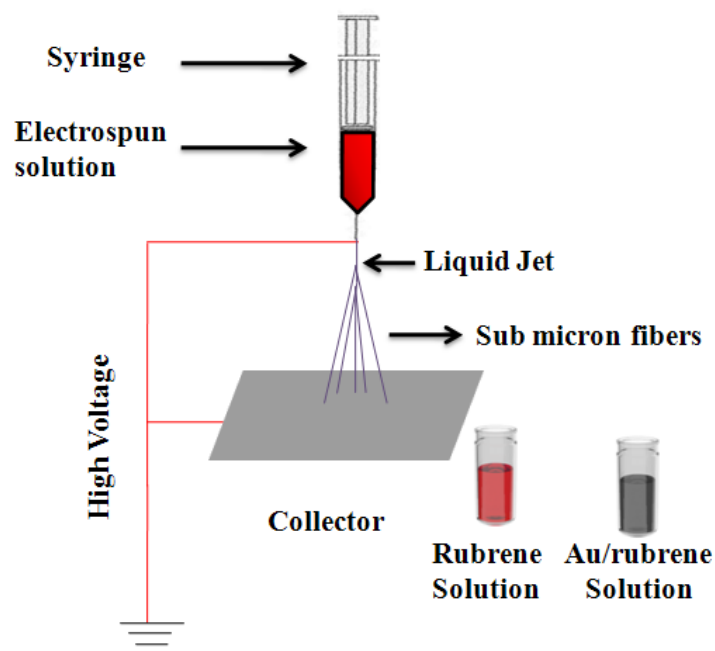


Fig. S₁: Schamatic of the electrospinning process of the rubrene NFs and hybrid NFs.

II. Porous size distribution on the hybrid rubrene NFs.

The porous size distribution is shown in the following bar diagram. The average size of the pores was ~500 nm and the coverage per NF is about ~10 %.

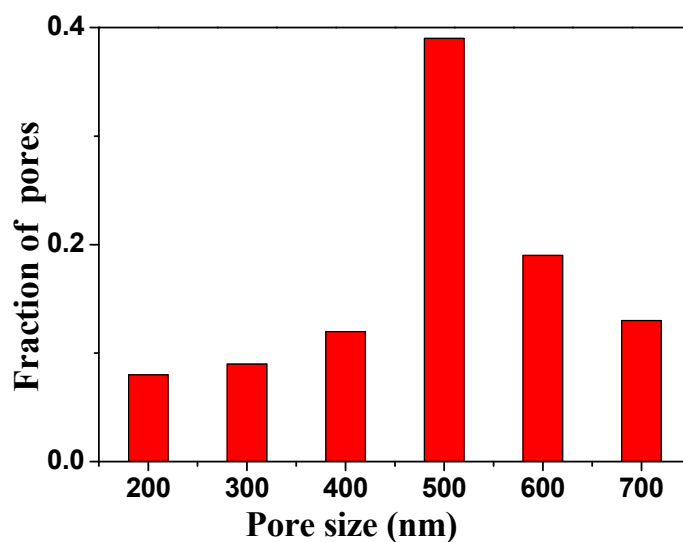


Fig. S₂: Porosity distribution on the hybrid rubrene NFs.

III. Finite difference time domain (FDTD) simulation result of the light absorption and scattering due to porous effect on the hybrid rubrene NFs.

Contribution to the total light extinction (scattered light and absorbed light) due to porous formation on the hybrid rubrene NF was investigated using commercial software Lumerical FDTD solutions. FDTD calculation provides the local electromagnetic field information such as the energy (wavelength), field amplitude and phase around the metal or dielectric nanostructures. Also one can obtain overall scattering and absorption spectra of arbitrary nanostructures. In this calculation, we used known values of refractive indexes (n , k) of rubrene material⁴, with the diameter of 500 nm. We designed otherwise the same two rubrene NF, one with porosity and the other without porosity. Size of the pores was designed as 70 nm diameter and 100 nm depth. Fig. S₃ shows the cross-section of electromagnetic field distribution of the NF without (a) and with (b) porosity. The field intensity around the rubrene

NFs do not show notable difference depending on the existence of designed porosity.

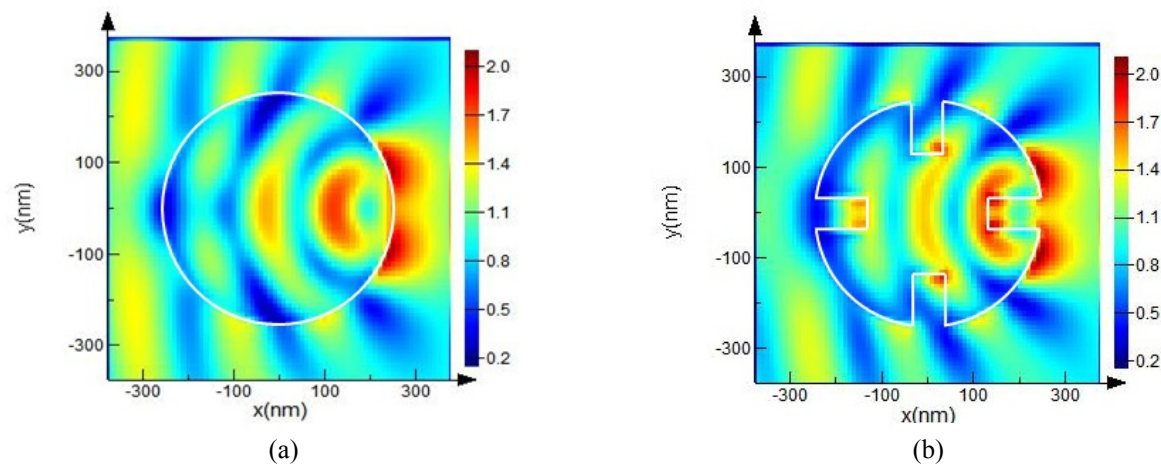


Fig. S3: FDTD simulation result of the field intensity around the cross-section of rubrene NF
(a) without and (b) with designed pores.

The total spectra of absorption and scattering are shown in the Fig. S4. The spectra are not normalized and thus can be compared directly in scattering and absorption strengths. The results show that there are slight increase in absorption and scattering in shorter wavelength range with the introduction of porosity on the rubrene NF, however overall differences of absorption and scattering strengths seem too small to give observed increase of optical extinction and PL intensity in hybrid NF.

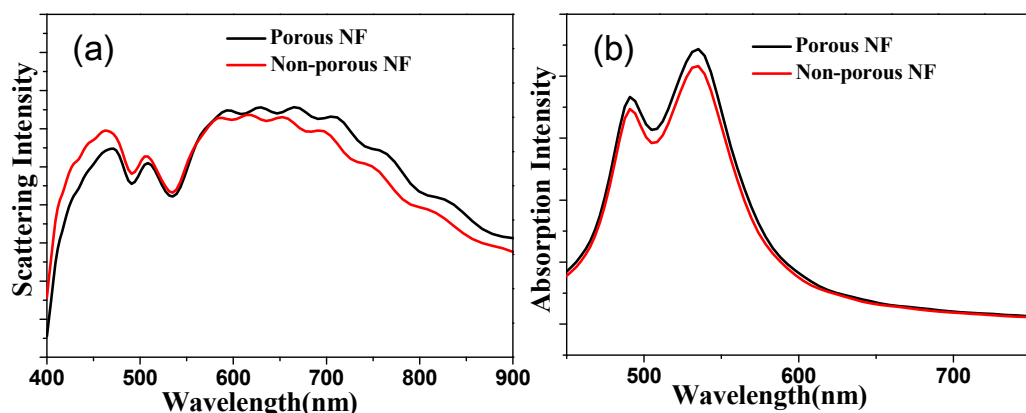


Fig. S4: FDTD simulation result of the light scattering (a) and absorption (b) that shows the

effect of porosity on the rubrene NFs.

IV. EDX analysis from the TEM image of the hybrid rubrene NF

The EDX analysis of the hybrid rubrene NFs is a very strong evidence to confirm the presence of nanoparticles in nm size, because a sub-nanometer size electron beam spot is used to analyse the elemental information. In our experiment, we took the EDX measurement of the hybrid rubrene NF, as the result shown in Fig. S₅, with an electron beam spot size of about 0.5 nm. Strong peaks of Au were observed in the spectrum confirming the presence of Au NPs in the hybrid rubrene NFs.

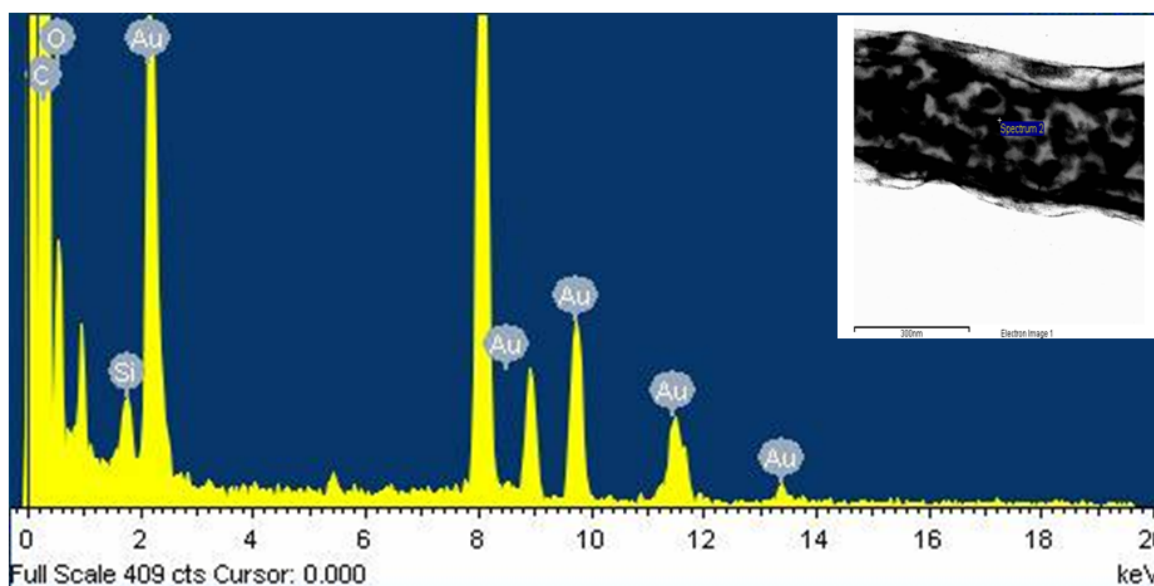


Fig. S₅: The EDX information of the hybrid NFs taken from the point shown in the inset of the TEM image. Strong peaks of Au are observed in the spectrum.

V. IR spectroscopy of rubrene NFs and hybrid NFs

IR spectroscopy is a powerful technique to identify the chemical compounds in their different phase or structures. In order to confirm the formation of rubrene NFs and hybrid NFs, we performed FT-IR spectroscopy, and characterized the vibrational bands of the

rubrene NFs and hybrid NFs, as the result shown in Fig. S₆. Experiments were carried out in vacuum condition, by directly putting a small amount of rubrene NF or hybrid NF collection on a Ge crystal.

The IR spectra of both rubrene NFs and hybrid NFs were found to be slightly different from the crystalline rubrene IR bands⁵, as shown in the Table 1. Assignment of IR bands of hybrid NFs with the IR bands of rubrene crystal confirmed the formation of rubrene NFs. We also assigned the IR bands of PEO and dodecanethiol functionalized Au NP from the rubrene NFs and hybrid NFs, as shown in the Table 1.

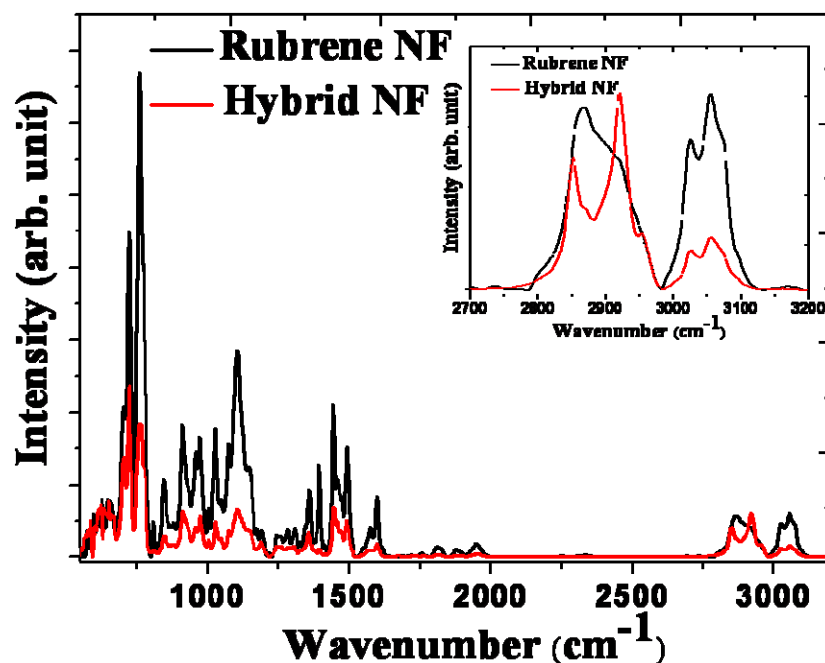


Fig. S₆: IR spectra of the rubrene NFs (black curve) and hybrid NFs (red curve); inset shows the presence of dodecanethiol capped Au NP in the hybrid rubrene NFs.

We have observed the difference in IR bands among rubrene NFs and hybrid NFs. This difference occurs due to the Au NP embedded inside the rubrene NFs, which may cause structural change in hybrid rubrene NF, as reported previously in the case of the Au/polymer

composite hybrid NFs.^{6,7} We clearly observed the presence of the dodecanethiol functionalized Au NP in the IR spectrum of the hybrid NFs at band positions of 2851, 2871, 2920 and 2955 cm⁻¹ as shown in the inset of the Fig. S₆, similar to the previously reported results of dodecanethiol functionalized Au NPs⁷⁻⁹. In the IR spectral features of thiols functionalized in Au NPs, CH₂ asymmetric and symmetric stretching bands are observed at 2918 and 2850 cm⁻¹, whereas in the spectrum of the free dodecanethiol IR band positions are observed at 2927 and 2855 cm⁻¹. This is due to the of trans zigzag conformation of alkyl chains onto the gold particle surface⁹.

Table 1. Peak positions of the IR bands from the rubrene NFs and hybrid rubrene NFs. Previously reported IR bands of rubrene single crystal,⁵ PEO,^{7,8} and dodecanethiol-functionalized Au NPs^{7,9} are also shown for comparison.

Rubrene crystal ⁵ (cm ⁻¹)	PEO ^{7,8} (cm ⁻¹)	Dodecanethiol-functionalized Au NPs ^{7,9} (cm ⁻¹)	rubrene NFs (cm ⁻¹)	hybrid NFs (cm ⁻¹)
695.9	-	-	702	702
720.0	-	-	725	725
754.1	-	-	757	757
768.6	-	-	771	771
-	-	-	808	810
846.3	842	-	841	845
911.3	-	-	909	909
-	961	-	958	958
967.7	-	-	971	971
1028.7	-	-	1026	1026
1069.4	-	-	1073	1073
-	1093	-	1104	1104
1148	1144	-	1145	1145
-	-	-	1190	1190
-	1240	-	1243	1243
-	1278	-	1281	1282
1309.5	-	-	1308	1301
-	1341	-	1342	-
-	-	-	1357	1357
-	-	1377	-	1377
1391.4	-	-	1393	1393
1412.5	-	1413	1413	1413
1438.8	-	-	1442	1442
-	1456	-	1455	1455
1464.3	1467	1466	1473	1469
1492.1	-	-	1492	1492
1556.3	-	-	1561	1562
1573.2	-	-	1574	1574
1597.1	-	-	1596	1596
1617.1	-	-	1617	-
1815.3	-	-	1813	1819
1881.2	-	-	1878	1880
1951.6	-	-	1949	1952
2333.0	-	-	2333	2338*
-	-	2850	-	2851
-	2863	-	2865	-
-	-	2871	-	2871
2925.5	-	2918	2924	2920
-	-	2955	-	2955
3022.7	-	-	3025	3025
3061.5	-	-	3055	3055

References

- 1 D. V. Leff, P. C. Ohara, J. R. Heath and W. M. Gelbart, *J. Phys. Chem.*, 1995, **99**, 7036.
- 2 M. S. Kim, D. H. Park, E. H. Cho, K. H. Kim, Q. H. Park, H. Song, D. C. Kim, J. Kim and J. Joo, *ACS Nano*, 2009 **3**, 1329.
- 3 K. P. Dhakal, H. Lee, J. W. Lee, J. Joo, M. Guthold and J. Kim, *J. Appl. Phys.*, 2012, **111**, 123504.
- 4 S. Tavazzi, A. Borghesi, A. Papagni, P. Spearman, L. Silvestri, A. Yassar, A. Camposeo, M. Polo and D. Pisignano, *Phys. Rev. B* 2007 **75**, 245416.
- 5 J. R. Weinberg-Wolf, Optical Characterization of Organic Semiconducting Single Crystals, *Ph.D Dissertation*, University of North Carolina, Chapel Hill, 2006, USA p 81.
- 6 C. A. E. Hamlett, S. N. Jayasinghe and J. A. Preece, *Tetrahedron*, 2008, **64**, 8476.
- 7 G. Kim, A. Wutzler, H. Radusch, G. H. Michler, P. Simon, R. A. Sperling and W. J. Parak, *Chem. Mater.*, 2005, **17**, 4949.
- 8 E. P. Enriquez and S. Granick, *Colloids and Surfaces A: Physicochemical and Engineering Aspects*, 1996, **113**, 11.
- 9 A. Manna, T. Imae, T. Yogo, K. Aoi and M. Okazaki, *J. Colloid Interface Sci.* 2002, **256**, 297.
- .